Mid- and far-infrared optical characterization of monoclinic HfO_2 nanoparticles and evidence of localized surface phonon polaritons

Owen Dominguez*[a], Tracie L. McGinnity[b], Ryan K. Roeder[b] and Anthony J. Hoffman[a]
[a]Department of Electrical Engineering, University of Notre Dame. Notre Dame, IN 46556 USA;
[b]Department of Aerospace and Mechanical Engineering, University of Notre Dame. Notre Dame, IN 46556 USA

ABSTRACT

Monoclinic HfO_2 nanoparticles (9 - 45 nm) are synthesized using a sol-gel method and optically characterized using transmission- and angle-dependent reflection spectroscopy in the mid- to far-infrared. A detailed HfO_2 identification of the infrared-active phonon modes is presented; consistent with previously reported thin film values, and in excellent agreement with density functional perturbation theory calculations. An anomaly is observed in both reflection and transmission measurements, at 556 cm^{-1} that is not attributed to the optical phonon modes. Numerical models indicate that this measured anomaly is in the spectral region of a localized surface phonon polariton mode. The results of this work suggest that HfO_2 nanoparticles could enable new mid- and far-infrared materials and devices with engineered optical properties.

Keywords: Nanoparticles, nanomaterials, surface polaritons

1. INTRODUCTION

Controlling light and engineering light-matter interactions on the nanoscale has revolutionized optics. The field of plasmonics, the study of the interaction between light and free-charge in materials, was born from these efforts. Plasmonics leverage sub-diffraction confinement of light and strong field enhancement to achieve extraordinary optical behavior. Noble metal nanoparticles (NPs) are one of the pillars of the field of plasmonics[1], and the excitation and control of highly-confined surface modes on NPs has enabled exquisite control of light at the nanoscale. Engineering the light-matter interactions via NP morphology, composition, organization, etc. has enabled new optical materials[2-4] and devices[5] and driven the development of applications in sensing and imaging[6,7] across the visible and near-infrared (near-IR). Unfortunately, NPs for mid- and far-infrared (mid-IR and far-IR, respectively) have lagged in development.

Localized modes, called localized surface plasmon polaritons (LSPPs) in plasmonics, are supported when the optical permittivity, ε, is negative and $|\varepsilon|$ is comparable to the surrounding dielectric[7]. For a material with free-charges, the permittivity depends on the free-charge density, n, and for noble metal NPs, n is very large, e.g., 5.9 x 10^{22} cm^{-3} for Au[8]. This large free-charge density results in $\epsilon \ll 0$ in the mid- and far-infrared. Figure 1 shows the permittivity of Au[9, 10] across the visible to far-IR. The red shaded region indicates where $-10 < \varepsilon < 0$. In the mid- and far-IR, the large, negative permittivity for noble metal NPs prevents the excitation of LSPPs. One strategy for engineering LSPPs at longer wavelengths is to reduce the free-charge density using doped semiconductors[11]. However, the preparation of doped semiconductor nanostructures—requiring high-temperature processes and nanolithography— is expensive and challenging compared with noble metal NPs. Furthermore, the permittivity of most semiconductor materials will ultimately be dominated by coupling to vibrations of the crystal lattice (phonons) in the mid- and far-infrared.

At wavelengths where the frequency of the incident light is similar to the frequency of optical phonons, light can couple to vibrations of the crystal lattice. For polar crystals, this coupling to the lattice is due to an electric dipole resulting from the charge separation between basis atoms in the primitive cell of the Bravais lattice[8]. In the long-wavelength IR, both free carriers and phonons can contribute significantly to the material's optical permittivity[12, 13]. The *Reststrahlen* band is the spectral region between the longitudinal optical and transverse optical phonons (LO and TO, respectively), where $\epsilon < 0$ even for an intrinsic material. Ultimately, Maxwell's Equations are indifferent to the source of the negative permittivity, and thus the negative permittivity resulting from phonon resonances in polar materials will support surface modes similar to LSPhPs. For polar materials, nanostructures and NPs made from these materials can support localized modes[12-15], called localized surface phonon polaritons (LSPhPs)[16] in the *Reststrahlen* band of the material.

Optical Components and Materials XIV, edited by Shibin Jiang, Michel J. F. Digonnet,
Proc. of SPIE Vol. 10100, 101001G · © 2017 SPIE · CCC code:
0277-786X/17/$18 · doi: 10.1117/12.2252844

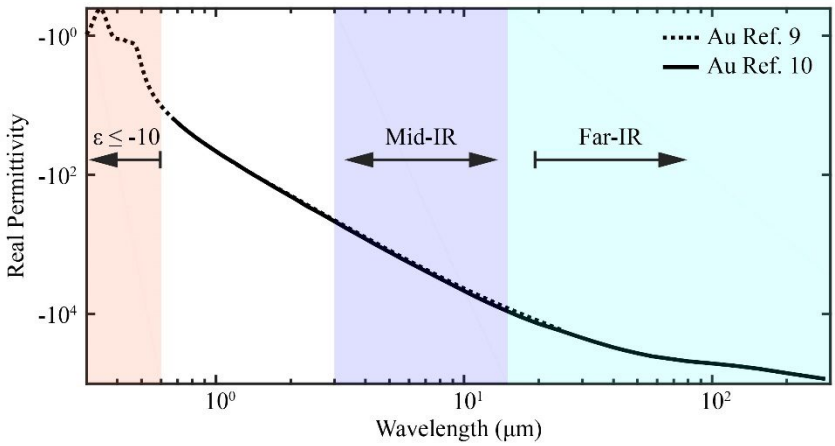

Figure 1. Real part of Au permittivity from Olmon[9] and Ordal[10]. Red shaded area indicates the permittivity range: $-10 < \varepsilon < 0$. Gold has a very large negative permittivity ($\epsilon \ll 0$) in the mid- to far-IR regions, also shaded blue and green, respectively.

Hafnium dioxide (HfO_2) is a polar crystal with a *Reststrahlen* band in the mid- and far-infrared. HfO_2 is already used in many photonic and electronic applications including optical coatings[17, 18], interference filters and dielectric mirrors[19-21], thermal barrier coatings[22, 23], and field-effect transistors[24, 25]. The *Reststrahlen* band of monoclinic HfO_2 (m-HfO_2) spans ~130-800 cm^{-1}. 15 infrared and 18 Raman active modes are predicted for m-HfO_2 using density functional perturbation theory (DFPT), and characterization of thin films shows good agreement between the predicted and measured optical phonon energies[26-28]. However, optical characterization of HfO_2 has thus far been limited to thin films[20, 22, 24, 29-32].

In this manuscript, we characterize monoclinic HfO_2 (m-HfO_2) NPs with nominal diameters of 9, 30 and 45 nm in the mid- to far-IR portion of the electromagnetic spectrum (250-1200 cm^{-1}). In the *Reststrahlen* band of m-HfO_2 we observe strong absorption from the IR active optical phonon modes. The frequencies of these modes agree well with the phonon energies predicted in the literature and previous measurements on thin films. Additionally, we observe an anomaly in the reflection and transmission measurements that is not explained by coupling to an optical phonon. We attribute this anomaly to coupling to a LSPhP on the HfO_2 NPs and present a model that supports this claim.

2. METHODS

HfO_2 NPs are synthesized by a sol-gel process, calcining a polymerized complex[34]. Aqueous reaction solutions are prepared by adding 0.208 M hafnium (IV) chloride, $HfCl_4$, to 24 mL of 2.08 M citric acid; the solutions are stirred overnight to ensure complete dissolution. Ethylene glycol (0.2 M) is then added to the solution under continuous stirring for 3 h at 90°C to boil off excess water. The resulting gel is calcined in a pre-heated furnace to pyrolize the remaining organics and crystallize HfO_2 NPs. The temperature and time of the calcination process determines the size of the NPs. Table 1 summarizes the nominal NP size, furnace temperature, and calcination time. The resulting HfO_2 powders are ground using a mortar and pestle prior to further preparations and characterization.

Table 1. HfO_2 NP synthesis parameters

Nominal diameter (nm)	Calcination Temperature (°C)	Calcination Time (h)
9	650	2
30	950	2
45	950	8

Thin films containing HfO_2 NPs are prepared on gold and KBr substrates for optical characterization. To create the thin films, HfO_2 NPs are surface functionalized with 1.5 – 2 wt% PVP and a suspension with 50 g/L of HfO_2 NPs in ethanol is prepared. For films on KBr substrates, which are appropriate for transmission measurements, suspension drops are placed over a 13 mm diameter KBr window using a pipette and spread using a wire-wound rod[33]. Samples for reflection measurements are prepared similarly using 2 x 2 cm^2 glass coverslips coated with a thin layer of Au. For both substrates, the NPs form films—as verified using scanning electron microscopy—with less than a monolayer of complete coverage.

In addition to the films containing NPs, KBr/HfO_2 pellets were also prepared with a total mass of 200 mg comprising of HfO_2 nanoparticles and KBr in a mass ratio of 1:200, respectively. The final thickness was measured as approximately 0.47-0.55 mm.

Angle-, wavelength-, and polarization-dependent transmission and reflection measurements are conducted from 250-7000 cm^{-1} using a Bruker Vertex 80 vacuum Fourier transform infrared spectrometer (FTIR). The measurements are performed in the internal sample compartment under vacuum to minimize atmospheric absorption. A standard globar and room-temperature DLaTGS detector are used for all of the measurements. KBr and Mylar beamsplitters are used for the mid- and far-infrared measurements, respectively, and a KRS-5 linear polarizer is used to select the transverse magnetic (TM) or transverse electric (TE) polarization of light. Spectra are collected using a resolution of 3 cm^{-1} and averaged over 200 scans. For angle-dependent reflection spectra, the VeeMAX III (PIKE Technologies) is used in the internal sample compartment.

3. RESULTS

3.1 Material Characterization

The size distributions of as-prepared HfO_2 NPs are obtained using transmission electron microscopy (TEM). Figure 2 shows the NP size distribution measured from 100 NPs for each synthesis (Table 1). The coefficient of variance (CV) is given by $CV=\sigma/\mu_d$, where σ and μ_d are the standard deviation and mean diameter, respectively, and are obtained using a Gaussian fit to the distribution (95% *confidence interval*: 9.05 ± 0.46 nm, 31.01 ± 1.66 nm, 43.80 ± 3.30 nm). HfO_2 NPs with a nominal diameter of 9, 30, and 45 nm exhibited a CV of 3.9, 3.7, and 2.6%, respectively. Additionally, agglomerates are present for all sizes but most noticeable in the 9 and 45 nm NPs. Therefore, in order to mitigate agglomeration, the NPs are coated with polyvinylpyrrolidone (PVP), vortexed, and sonicated several times to ensure dispersion.

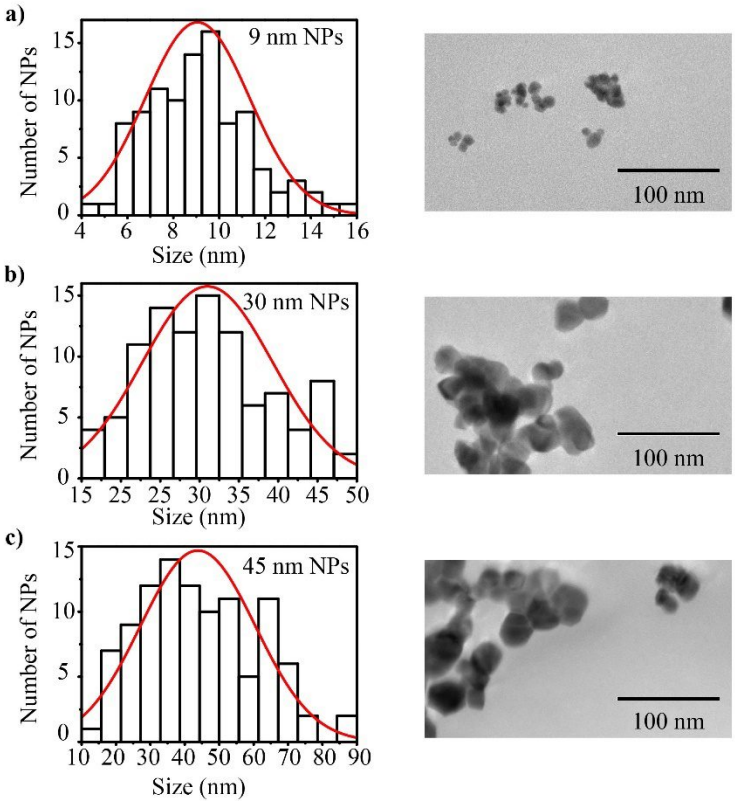

Figure 2. Measured NP size distribution for HfO_2 NPs with a nominal diameter of (a) 9 nm, (b) 30 nm, and (c) 45 nm, and corresponding representative TEM micrographs.

Coverage on the Au and KBr substrates is evaluated qualitatively using scanning electron microscopy (SEM). Panels (a), (b) and (c) in Figure 3 show coverage for the 9, 30 and 45 nm NPs on an Au-coated glass slide, respectively. In Figure 3a) several large agglomerations of 9 nm NPs are visible. The diagonal lines are grooves in the gold from the wire wound rod. Figure 3 (b) is a higher magnification image taken in between parallel grooves for a sample comprising 30 nm NPs. The spatial coverage is low and agglomeration of the NPs is still evident. The degree of spatial coverage is controlled using the concentration of NPs in the suspension and the type of wire wound rod. Figure 3 (c) is a higher magnification image of a 45 nm NPs agglomeration.

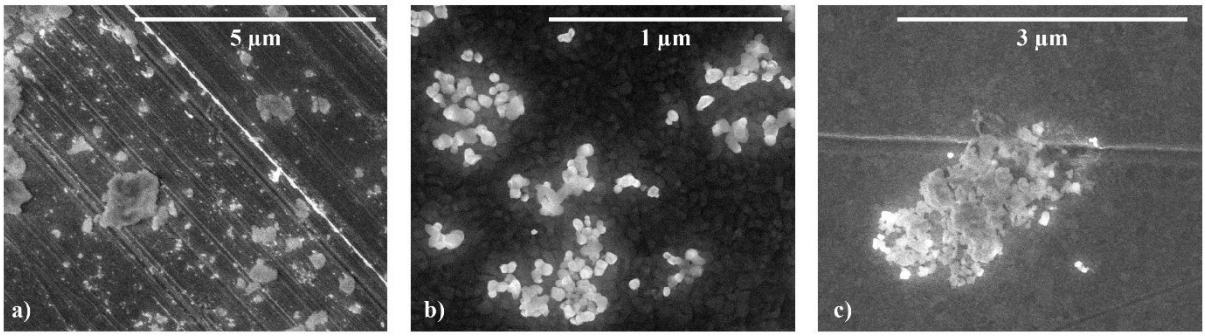

Figure 3. SEM images showing for samples comprising 9, 30 and 45 nm NPs on an Au-coated glass slide, respectively. (a) several large agglomerations of 9 nm NPs are visible. The diagonal lines are grooves in the gold from the wire wound rod. (b) image taken in between parallel grooves for a sample with 30 nm NPs. c) image of a 45 nm NPs agglomeration.

The crystalline structure of the synthesized NPs is determined using Raman spectroscopy and X-ray diffraction (XRD). The Raman active modes are measured using micro-Raman on NPs deposited on a glass substrate. Figure 4 (a) shows the measured Stokes component of the scattered light. Sixteen peaks are visible in the measured spectrum while eighteen modes are predicted from DFPT calculations (9 A_g and 9 B_g) for m-HfO_2[26-28]. We account for the difference by noting that at 139 cm^{-1} the A_g and B_g modes are degenerate and the small frequency difference for the modes at 326 and 336 cm^{-1} results in a single, broadened peak. Figure 4 (b) shows the results of XRD measurements. All measured XRD peaks correspond to m-HfO_2[34]. Combined, the Raman and XRD measurements indicate that the synthesized NPs are m-HfO_2.

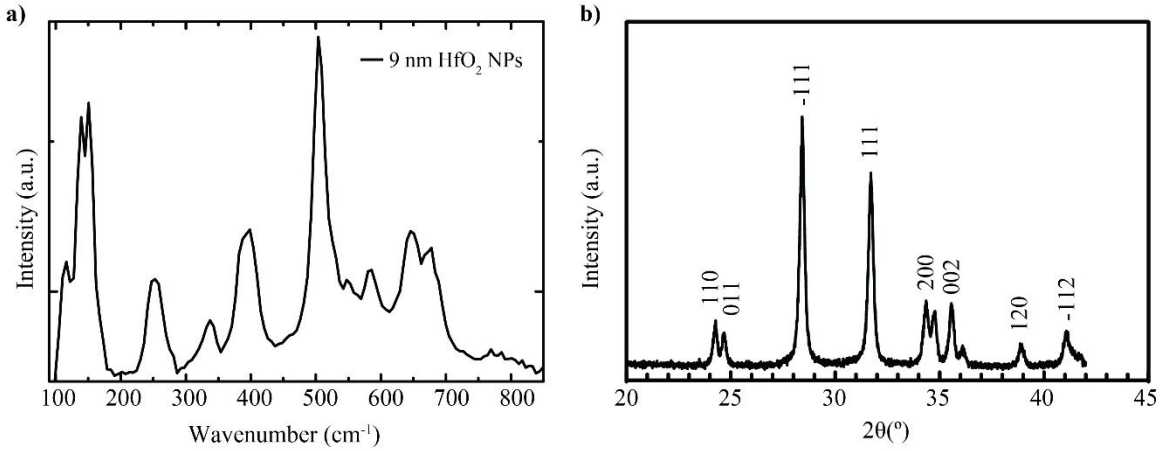

Figure 4. (a) Stokes Raman shift spectrum and (b) powder XRD pattern for HfO_2 NPs with a nominal diameter of 9 nm.

3.2 Optical Characterization

Angle-dependent reflectance spectra for TM polarized light are depicted in Figure 5 (a) for NPs with nominal diameters of 30 nm. All of the spectra exhibit dips at frequencies below 850 cm^{-1} and a monotonic decrease in reflectance beyond 850 cm^{-1}. At low frequencies, the dips are primarily due to optical phonon modes in the NP, and we attribute the high-frequency behavior to Rayleigh scattering effects. While the decrease with increasing frequency does not follow the

expected λ^{-4} dependence, similar effects have been reported in the mid-infrared region with Si NPs of comparable size[35], and the deviation from the expected behavior is attributed to the complex NP-NP and NP-substrate interactions, coating effects of the PVP, and KBr window.

Figure 5 (b) shows the transmission spectra of 60 nm NPs using KBr pellets. Although, there was little difference of the transmission measurements between the KBr pellets and KBr surface coated with NPs, the latter is chosen for the subsequent analysis, because of the ability to control NPs dispersion and thickness of the layer of nanoparticles on the substrate.

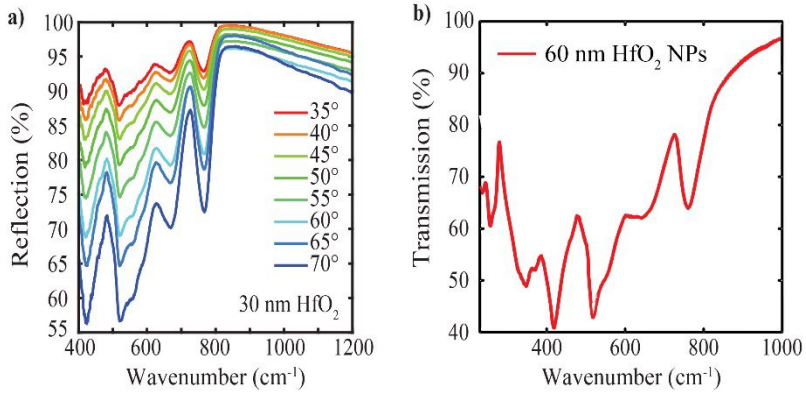

Figure 5. (a) Reflection measurement of 30 nm HfO_2 NPs at various angles of incidence under TM light illumination. The reflected surface is composed of HfO_2 NPs dispersed on top of a gold mirror surface. (b) Transmission measurement using KBr/HfO_2 NP pellets for 60 nm NPs.

The majority of the dips in the reflection and transmission spectra can be understood by considering the optical phonon modes. In general, dips in the transmission correspond to absorption by a phonon mode at the center frequency of the dip. 15 IR-active phonon modes are expected for m-HfO_2 and their resonance frequency, oscillator strength, and damping constant can be estimated using DFPT[26]. In our transmission measurements, there is a low-energy cutoff due to strong absorption in the KBr substrate. Therefore, we do not expect to see the lowest energy phonon mode predicted in[18]; however, all other modes are visible. For the measured transmission shown in Figure 6 (a). The vertical dashed lines indicate optical phonon frequencies as predicted using DFPT from Ref. 26. The shaded red regions centered about each vertical line indicate error bars of ±5%.

To identify the various spectral features, we fit the measured transmission data with a simulated curve that is calculated using transfer matrix code with a multiple-oscillator model for the permittivity of the thin film[36]. The transfer matrix model treats the NPs as a thin film and is appropriate for determining the frequency, oscillator strength, and damping constant. The effective permittivity in the mid- to far-IR is described using the following equation:

$$\varepsilon(\omega) = \varepsilon_\infty + \sum_j \frac{\omega_{pj}^2}{\omega_j^2 - \omega^2 - i\gamma_j\omega} \quad (1)$$

where ε_∞ is the high frequency limit dielectric constant; the sum is over all IR-active optical phonon modes; ω_j, ω_{pj}, and γ_j are the resonance frequency, plasma frequency, and damping constant of the j-th oscillator, respectively. We use ε_∞, ω_j, ω_{pj}, and γ_j as fitting parameters and limit the range of ω_j to ±5% of the predicted phonon energies in Ref. 26 in the fitting algorithm. Table 2 summarizes the identified HfO_2 IR phonon modes from literature[26], and the recovered fitting parameters obtained using a least squares method with the measured transmission and the simulated transmission obtained using the transfer matrix code.

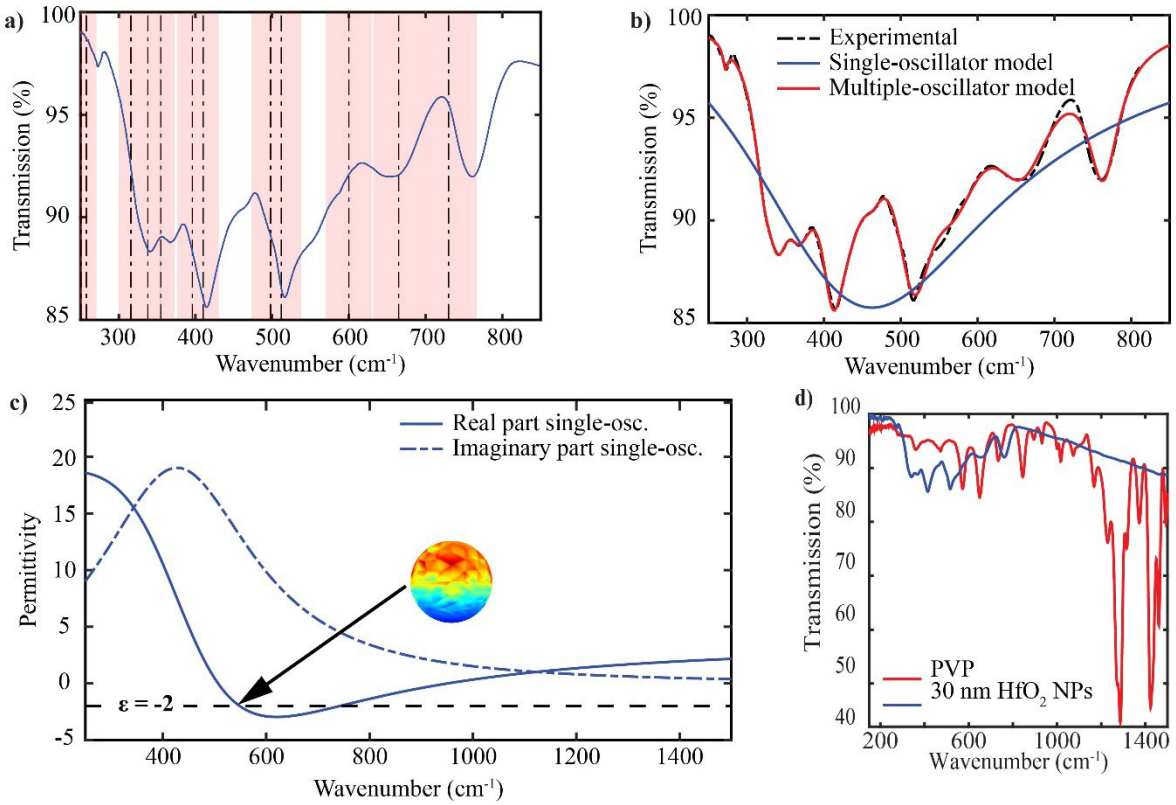

Figure 6. (a) Identified phonon modes of HfO_2 NPs (dashed lines) showing 5% error bars (shaded). Most absorption dips can be aligned with a phonon mode. (b) Experimental transmission from 30 nm HfO_2 NPs (black line), fitting using transfer matrix method and a multiple-oscillator model of a 30 nm effective thin film (red line), and fitting using a single-oscillator model (blue line). (c) Real and imaginary parts of the permittivity recovered using a least squared regression method, for single-oscillator models. (d) Transmission comparison of 30 nm HfO_2 NPs coated with 5% PVP versus PVP alone.

Figure 6 (b) shows the calculated transmission using the recovered effective permittivity (Eq. 1) superimposed on the experimental transmission. A single-oscillator model that uses a single LO and TO phonon is also shown. There is excellent agreement between the measurement and multiple-oscillator model over the majority of the spectral region; however, there is some deviation around 556 cm^{-1}. As seen in Fig. 6 (a) and Table 1, no optical phonons are predicted in this portion of the spectrum. Furthermore, the phonons that are energetically close to the anomalous region describe observed dips in the transmission. Attributing this anomaly to a phonon is not consistent with the already strong agreements between our measurements and previously published results—both experiment and theory.

We attribute this anomaly in transmission at around 556 cm^{-1} to LSPhPs coupling on the NPs. This localized mode is the so-called Fröhlich mode[37], which is a homogeneous vibrational surface mode in spherical NPs. The Fröhlich mode makes itself evident in NPs at $\varepsilon = -2$. In order to support our claim regarding HfO_2 NPs coupling to LSPhPs, we regressively calculate the NPs effective permittivity. We assume that the nanoparticles from an isotropic medium (thin film) and use a single-oscillator model fit to the transmission data. Figure 6 (c) shows the recovered permittivity using the single-oscillator model that was fit to the experiment transmission (Fig. 6 (b)).

Table 2. Modified parameters for multiple-oscillator model of HfO_2

Phonon frequency from Ref. [25] (cm^{-1})	Resonance frequency from fit, ω_j (cm^{-1})	Plasma frequency, ω_{pj} (cm^{-1})	Damping constant, γ_j (cm^{-1})
251	238	50	170
258	272	60	8
316	323	273	32
338	340	340	345
355	369	424	50
396	412	380	36
410	430	481	71
498	463	196	36
512	517	566	58
600	570	535	90
665	658	543	95
730	763	410	48

In addition, we analytically calculate the LSPhP frequency. For this calculation, however, we use reported HfO_2 thin film values[29]. The TO and LO optical phonon frequencies are estimated as ω_{TO} = 336.7 cm^{-1} and ω_{LO} = 662 cm^{-1}, respectively. Then, the frequency of the LSPhP for an isotropic NP surrounded by a dielectric is given by[37]:

$$\omega_{LSPhP} = \sqrt{\omega_{TO}^2 \frac{\varepsilon_0 + \varepsilon_{m(2)}}{\varepsilon_\infty + \varepsilon_{m(2)}}} \quad (2)$$

where ε_∞ = 3.74 and ε_0 = 17 - 25[38] are the high frequency limit dielectric constant and the static dielectric constant of HfO_2, respectively, and ε_m = 2.33 is the KBr dielectric constant[35]. Using the values above, the frequency of the LSPhP is varies between 541 - 632 cm^{-1} for different values of ε_0. When ε_0 = 18, ω_{LSPhP} = 553 cm^{-1}, which is close to the value of the anomaly observed on the 30 nm NPs. We also perform finite element calculations using COMSOL Multiphysics. Using the same single-oscillator effective permittivity, the models predict LSPhPs at frequencies similar to Eq. (2). The inset of Figure 6 (c) shows the charge density on the HfO_2 NPs at 553 cm^{-1} and for ε_0 = 18. The blue and red regions indicate negative and positive charge, respectively. The charge density has the characteristic dipolar nature expected for the Fröhlich mode[39]. The numerical models predict a stronger deviation in reflection and transmission on the spectrum. We attribute the weaker anomaly observed in experiment to non-ideal dispersion of the NPs. Finally, we only observe this anomaly for the 30 nm NPs prepared as thin films. We believe that coupling to the LSPhP is not observed for the 9 and 45 nm NPs due to poor dispersion of the NPs during the preparation of thin films, which was confirmed by SEM. Similarly, the anomaly is not observed in the HfO_2/KBr pellets due to the increased density of NPs and the resulting spectral shifts and broadenings associated with coupling between closely packed NPs.

Finally, to verify that the spectral anomaly is not due to the PVP coating, we measure transmission through a thin layer of PVP on a KBr window. The transmission spectrum, Figure 6 (d), exhibits absorption bands in between 200 and 2000 cm^{-1}; however, none of these features are present in the transmission measurements of the NPs and none of the spectral features occur at the same frequency as the anomaly.

4. CONCLUSIONS

HfO_2 NPs are synthesized using a sol-gel method with nominal diameters of 9, 30 and 45 nm and are optically characterized across the mid- and far-infrared. The crystal structure of the NPs is identified as monoclinic using Raman spectroscopy and XRD. Angle-dependent reflection and transmission measurements of the NPs exhibit dips that correspond to the optical phonon modes of m-HfO_2. An anomaly that cannot be attributed to an optical phonon is observed at 556 cm^{-1}. We argue that the observed anomaly is present as a result of the NPs coupling to a LSPhP mode. To support this claim, we introduce a simple numerical model that predicts LSPhP modes around this frequency, 553 cm^{-1}. This work demonstrates the potential for using polar crystals NPs in the mid- and far-IR as an analog of noble metal NPs in the visible. These polar NPs could lead to improved sensing and materials for this important part of the spectrum.

5. ACKNOWLEDGMENTS

This work is supported in part by funding from DARPA (FA8650-15-C-7546), NSF (ECCS-1609362), and NSF (DMR-1309587).

REFERENCES

[1] Halas, N. J. "Plasmonics: an emerging field fostered by Nano Letters," Nano Lett. **10**, 3816 (2010).
[2] Engheta, N. "Circuits with light at nanoscales: Optical nanocircuits inspired by metamaterials," Science **317**, 1698-1702 (2007).
[3] Li, Z., Butun, S. & Aydin, K. "Touching Gold Nanoparticle Chain Based Plasmonic Antenna Arrays and Optical Metamaterials," ACS Photonics **1**, 228-234 (2014).
[4] Sandu, T., Vrinceanu, D. & Gheorghiu, E. "Surface Plasmon Resonances of Clustered Nanoparticles," Plasmonics **6**, 407-412 (2011).
[5] Chen, J., Sun, C. & Hu, X. "Nanoscale all-optical devices based on surface plasmon polaritons," Chin. Sci. Bull. **59**, 2661-2665 (2014).
[6] F. Verger, T. Pain, V. Nazabal, C. Boussard-Plédel, B. Bureau, F. Colas, E. Rinnert, K. Boukerma, C. Compère, M. Guilloux-Viry, S. Deputier, A. Perrin, J.P. Guin, "Surface enhanced infrared absorption (SEIRA) spectroscopy using gold nanoparticles on As2S3 glass," Sens. Actuators B: Chem., **175**, 142-148 (2012).
[7] Willets, K. A. & Van Duyne, R.,P. "Localized surface plasmon resonance spectroscopy and sensing," Annu. Rev. Phys. Chem. **58**, 267 (2007).
[8] Ashcroft, N. W., Mermin, N. D. [Solid State Physics]. Holt, Rinehart and Winston, New York, (1976).
[9] Olmon, R., Slovick, B., Johnson, T., Shelton, D., Oh, S., Boreman, G., & Raschke, M. "Optical dielectric function of gold". Phys. Rev. B **86**, (2012).
[10] Ordal, M. A., Bell, R. J., Alexander, R. W., Long, L. L. & Querry, M. R. "Optical properties of Au, Ni, and Pb at submillimeter wavelengths," Appl. Opt. **26**, 744 (1987).
[11] Law, S., Adams, D. C., Taylor, A. M. & Wasserman, D. "Mid-infrared designer metals," Opt. Express **20**, 12155-12165 (2012).
[12] Caldwell, J., Lindsay, L., Giannini, V., Vurgaftman, I., Reinecke, T., Maier, S., Glembocki, O. "Low-loss, infrared and terahertz nanophotonics using surface phonon polaritons," Nanophotonics **4**, 44-68 (2015).
[13] Feng, K., Streyer, W., Zhong, Y., Hoffman, A. J. & Wasserman, D. "Photonic materials, structures and devices for Reststrahlen optics," Opt. Express **23**, A1418 (2015).
[14] Feng, K., Streyer, W., Islam, S., Verma, J., Jena, D., Wasserman, D., Hoffman, A., "Localized surface phonon polariton resonators in GaN," OSA, CLEO: 2015.
[15] Streyer, W., Law, S., Rosenberg, A., Roberts, C., Podolskiy, V. A., Hoffman, A., Wasserman, D., "Engineering absorption and blackbody radiation in the far-infrared with surface phonon polaritons on gallium phosphide," Appl. Phys. Lett. **104** (2014).
[16] Chen, Y., Francescato, Y., Caldwell, J. D., Giannini, V., Maß, T. W. W., Glembocki, O. J., Bezares, F. J., Taubner, T., Kasica, R., Hong, M., Maier, S. A. "Spectral tuning of localized Surface phonon polariton resonators for low-loss mid-IR applications," ACS Photonics **1**, 718-724 (2014).
[17] Tokas, R. B., Jena, S., Thakur, S. & Sahoo, N. K. "Effect of angle of deposition on micro-roughness parameters and optical properties of HfO2 thin films deposited by reactive electron beam evaporation," Thin Solid Films **609**, 42-48 (2016).
[18] Lehan, J. P., Mao, Y., Bovard, B. G. & Macleod, H. A. "Optical and microstructural properties of hafnium dioxide thin films," Thin Solid Films **203**, 227-250 (1991).
[19] Jiao, H., Cheng, X., Bao, G., Han, J., Zhang, J., Wang, Z., Trubetskov, M., Tikhonravov, A. V., "Study of HfO_2/SiO_2 dichroic laser mirrors with refractive index inhomogeneity," Appl. Opt. **53**, A56-A61 (2014).
[20] Smalakys, L., Bataviciute, G., Pupka, E. & Melninkaitis, A. "Comprehensive studies of IR to UV light intensification by nodular defects in HfO_2/SiO_2 multilayer mirrors," Laser-Induced Damage in Optical Materials **9237**, 92371I (2014).

[21] Wang, J., Schroeder, S., Trost, M., Hauptvogel, M. & Duparre, A. "Angle Resolved Backscatter of HfO_2/SiO_2 Multilayer Mirror at 1064 nm," Window and Dome Technologies and Materials XIV, **94530T** (2015).
[22] Matsumoto, K., Itoh, Y. & Kameda, T. "EB-PVD process and thermal properties of hafnia- based thermal barrier coating," Sci. Technol. Adv. Mater. **4**, 153-158 (2003).
[23] Wang, J., Li, H. & Stevens, R. "Hafnia and hafnia-toughened ceramics," J. Mater. Sci. **27**, 5397-5430 (1992).
[24] Fiorentini, V. & Gulleri, G. "Theoretical evaluation of zirconia and hafnia as gate oxides for Si microelectronics," Phys. Rev. Lett. **89**, 266101 (2002).
[25] Moldovan, C., Iosub, R., Modreanu, M., Ulieru, D., Firtat, B., Ion, M., "ISFET microsensors HfO_2 Based for Biomedical Applications," International Semiconductor Conference **1**, 185-188 (2006).
[26] Wu, R., Zhou, B., Li, Q., Jiang, Z., Wang, W., Ma, W., Zhang, X., "Elastic and vibrational properties of monoclinic HfO_2 from first- principles study," J. Phys. D: App. Phys. **45**, 125304 (2012).
[27] Zhou, B., Shi, H., Zhang, X. D., Su, Q. & Jiang, Z. Y. "The simulated vibrational spectra of HfO_2 polymorphs," J. Phys. D: App. Phys. **47**, 115502 (2014).
[28] Zhao, X. & Vanderbilt, D. "First- principles study of structural, vibrational, and lattice dielectric properties of hafnium oxide," Phys. Rev. B **65** (2002).
[29] Bright, T. J., Watjen, J. I., Zhang, Z. M., Muratore, C. & Voevodin, A. A. "Optical properties of HfO2 thin films deposited by magnetron sputtering: From the visible to the far-infrared," Thin Solid Films **520**, 6793-6802 (2012).
[30] Franta, D., Ohlídal, I., Nečas, D., Vižd'a, F., Caha, O., Hasoň, M., Pokorný, P., "Optical characterization of HfO_2 thin films," Thin Solid Films **519**, 6085-6091 (2011).
[31] Martínez, F. L., Toledano-Luque, M., Gandía, J. J., Cárabe, J., Bohne, W., Röhrich, J., Strub, E., Mártil, I., "Optical properties and structure of HfO_2 thin films grown by high pressure reactive sputtering," J. Phys. D: App. Phys. **40**, 5256-5265 (2007).
[32] Al-Kuhaili, M. "Optical properties of hafnium oxide thin films and their application in energy-efficient windows," Opt. Mater. **27**, 383-387 (2004).
[33] Jeong, S., Hu, L., Lee, H. R.., Garnett, E., Choi, J. W., Cui, Y. J., "Fast and scalable printing of large area monolayer nanoparticles for nanotexturing applications," Nano Lett. **10**, 2989 (2010).
[34] Mcginnity, T. L., Dominguez, O., Curtis, T. E., Nallathamby, P. D., Hoffman, A. J., Roeder, R. K., "Hafnia (HfO_2) nanoparticles as an X-ray contrast agent and mid-infrared biosensor," Nanoscale (2016).
[35] Kravets, V. G., Meier, C., Konjhodzic, D., Lorke, A. & Wiggers, H. "Infrared properties of silicon nanoparticles," J. Appl. Phys. **97** (2005).
[36] Bohren, C. F. & Huffman, D. R. [Absorption and scattering of light by small particles], Wiley, New York, (1983).
[37] Roca, E., Trallerogíner, C. & Cardona, M. "Polar optical vibrational- modes in quantum dots," Phys. Rev. B **49**, 13704-13711 (1994).
[38] Bundesmann, C., Buiu, O., Hall, S. & Schubert, M. "Dielectric constants and phonon modes of amorphous hafnium aluminate deposited by metal organic chemical vapor deposition," Appl. Phys. Lett. **91** (2007).
[39] Zhang, Q. & Zhang, Z. "Surface mode absorption and infrared optical properties of gallium phosphide nanoparticles," Appl. Phys. A **91**, 631-635 (2008).